Available online at www.sciencedirect.com
ScienceDirect
Journal of Sound and Vibration 318 (2008) 176–192
JOURNAL OF SOUND AND VIBRATION
www.elsevier.com/locate/jsvi

Free vibration analysis of functionally graded curved panels using a higher-order finite element formulation

S. Pradyumna*, J.N. Bandyopadhyay

Department of Civil Engineering, Indian Institute of Technology, Kharagpur, West Bengal 721 302, India

Received 31 July 2007; received in revised form 8 February 2008; accepted 30 March 2008
Handling Editor: Prof. L.G. Tham
Available online 27 May 2008

Abstract

Free vibration analysis of functionally graded curved panels is carried out using a higher-order formulation. A C^0 finite element formulation is used to carry out the analysis. The element consists of nine degrees of freedom per node with higher-order terms in the Taylor's-series expansion, which represents the higher-order transverse cross-sectional deformation modes. The formulation includes Sanders' approximation for doubly curved shells considering the effects of rotary inertia and transverse shear. A realistic parabolic distribution of transverse shear strains through the shell thickness is assumed and the use of shear correction factor is avoided. Material properties are assumed to be temperature independent and graded in the thickness direction according to a simple power-law distribution in terms of the volume fractions of the constituents. Heat conduction between ceramic and metal constituents is neglected. The accuracy of the formulation is validated by comparing the results with those available in the literature. Effects of panel geometry parameters and boundary conditions are studied.

1. Introduction

Functionally graded materials (FGM) are heterogeneous composite materials usually made from a mixture of metals and ceramics. The material properties of FGM are graded but continuous and are controlled by the variation of the volume fraction of the constituent materials. A group of material scientists in Japan introduced the concept of FGM in 1984 as ultrahigh temperature-resistant materials for aircraft, space vehicles and other applications. FGM are now being strongly considered as a potential structural material for future high-speed spacecraft. With the increased use of these materials, it is important to understand the behavior of functionally graded (FG) plates and shells. Fukui and Yamanaka [1] studied the elastic problem of thick walled FG tubes subjected to internal pressure. Buckling of FG hybrid composite plates was studied by Birman [2]. Aboudi et al. [3] developed a Cartesian coordinate based higher-order theory for FGMs, which circumvents the problematic use of the standard micromechanical approach, based on the concept of a representative volume element, commonly employed in FG composites. Reddy [4] obtained Navier's solutions

*Corresponding author. Tel.: +91 3222 283404; fax: +91 3222 282254.
E-mail addresses: pradyumna@civil.iitkgp.ernet.in (S. Pradyumna), jnb@civil.iitkgp.ernet.in (J.N. Bandyopadhyay).

0022-460X/$ - see front matter © 2008 Elsevier Ltd. All rights reserved.
doi:10.1016/j.jsv.2008.03.056

and finite element results based on the third-order shear deformation theory for FG plates. Sankar [5] obtained an elasticity solution for FG beams considering exponential variation of elastic properties through the thickness. Woo and Meguid [6] carried out nonlinear bending analysis of FG plates and shallow shells subjected to transverse mechanical load and a temperature field. Chakraborty et al. [7] developed a new beam element for analyzing FGMs. A hierarchic family of finite elements for analyzing Reissner–Mindlin FG plates based on the ad hoc variational formulation was presented by Croce and Venini [8]. Bhangale and Ganesan [9] carried out static analysis of simply supported FG and layered magneto-electro-elastic plates. Nonlinear bending analysis of simply supported FG plates subjected to transverse loading in thermal environment was carried out by Shen [10] and GhannadPour and Alinia [11] investigated large deflection behavior of FG plates under pressure loads.

Many researchers studied dynamic behavior of FGM structures in the past few years. Praveen and Reddy [12] investigated the nonlinear transient thermoelastic behavior of FG ceramic-metal plates and found that, in general, the response of plates with material properties between those of ceramic and metal is not intermediate to the responses of the ceramic and metal plates. Loy et al. [13] studied the free vibration of simply supported FG cylindrical shells. Pradhan et al. [14] studied the effect of different boundary conditions on the natural frequencies of FG cylindrical shells made up of stainless steel and zirconia. Influence of the volume fractions and the effects of configurations of the constituent materials on the parametric instability regions of FG plates were investigated by Ng et al. [15]. Dynamic stability of simply supported FG cylindrical shells under harmonic axial loading was analyszd by Ng et al. [16] using a normal mode expansion and Bolotin's method to determine the boundaries of instability. Yang and Shen [17] investigated the free and forced vibration characteristics of shear deformable initially stressed FG plates in thermal environment. By considering the material properties of the constituents to be nonlinear functions of the temperature and graded in the thickness direction by power law distribution, Yang and Shen [18] investigated the free vibration and parametric resonance of shear deformable FG cylindrical panels. Patel et al. [19] carried out the free vibration analysis of FG elliptical cylindrical shells using a higher-order theory. Nonlinear free vibration behavior of FG plates was investigated by Woo et al. [20].

Liew et al. [21] dealt with the linear and nonlinear vibration analysis of a three-layer coating FGM substrate cylindrical panel with general boundary conditions and subjected to a temperature gradient across the thickness. Chen [22] presented the nonlinear partial differential equations of nonlinear vibration for a FG plate in a general state of non-uniform initial stress state. Huang and Shen [23] studied the nonlinear vibrations and dynamic response, and Sundararajan et al. [24] investigated the nonlinear free flexural vibrations of FG rectangular and skew plates in thermal environments, respectively. Huang and Shen [25] dealt with the nonlinear vibration and dynamic response of a FGM plate with surface-bonded piezoelectric layers in thermal environment. Postbuckling of axially loaded FG cylindrical panels with piezoelectric actuators in thermal environments was studied by Shen and Liew [26]. Thermo-mechanical postbuckling of FGM cylindrical panels with temperature-dependent properties was investigated by Yang et al. [27] and Shen and Leung [28]. Kim [29] developed a theoretical method to investigate vibration characteristics of initially stressed FG plates in thermal environment. Thermal postbuckling and vibration behavior of the FG plates were studied by Park and Kim [30]. Kadoli and Ganesan [31] presented linear thermal buckling and free vibration analyses of clamped–clamped FG cylindrical shells based on temperature-dependent material properties. Shen and Noda [32] presented the theoretical postbuckling analysis of shear deformable FGM cylindrical shells subjected to combined axial and radial mechanical loads in thermal environments using a higher-order shear deformation shell theory.

Several investigators also developed higher-order theories in which the displacements of the middle surface are expanded as cubic functions of the thickness coordinate and the transverse displacement is assumed to be constant through the thickness. This displacement field leads to the parabolic distribution of the transverse shear stresses and, therefore, the use of shear correction factors is avoided. To the best of the authors' knowledge, however, limited literature is available related to the application of higher-order theory for studying the free vibration behavior of FG curved panels and the authors attempt to fill this lacuna is first of its kind and new. Therefore, in the present analysis, free vibration of FG curved panels is studied by employing the higher-order shear deformation theory (HSDT) developed by Kant and Khare [33] by including the twist curvature using the finite element method. Material properties are assumed to be temperature independent and heat conduction between ceramic and metal constituents is neglected.

2. Mathematical formulation

Let us consider a shell element made of a FG material with the coordinate (x, y, z) as shown in Fig. 1. The coordinate system (x, y, z) is chosen such that the plane x–y at $z = 0$ coincides with the mid-plane. In order to approximate the three-dimensional (3-D) elasticity problem to a two-dimensional (2-D) one, the displacement components $u(x, y, z)$, $v(x, y, z)$ and $w(x, y, z)$ at any point in the shell space are expanded in Taylor's series in terms of the thickness coordinate. The elasticity solution indicates that the transverse shear stresses vary parabolically through the element thickness. This requires the use of a displacement field in which the in-plane displacements are expanded as cubic functions of the thickness coordinate. The displacement fields, which satisfy the above criteria are assumed in the form as given by Kant and Khare [33]

$$\begin{aligned} u(x,y,z) &= u_0(x,y) + z\theta_y + z^2 u_0^*(x,y) + z^3\theta_y^*(x,y) \\ v(x,y,z) &= v_0(x,y) - z\theta_x + z^2 v_0^*(x,y) - z^3\theta_x^*(x,y) \\ w(x,y,z) &= w_0 \end{aligned} \tag{1}$$

where u, v and w are the displacements of a general point (x, y, z) in an element along x, y and z directions, respectively. The parameters u_0, v_0, w_0, θ_x and θ_y are the displacements and rotations of the middle plane, while u_0^*, v_0^*, θ_x^* and θ_y^* are the higher-order displacement parameters defined at the mid-plane.

The linear strain–displacement relations according to Sanders' approximation are

$$\begin{aligned} &\varepsilon_x = \frac{\partial u}{\partial x} + \frac{w}{R_x}, \quad \varepsilon_y = \frac{\partial v}{\partial y} + \frac{w}{R_y}, \quad \gamma_{xy} = \frac{\partial v}{\partial x} + \frac{\partial u}{\partial y} + \frac{2w}{R_{xy}}, \\ &\gamma_{xz} = \frac{\partial u}{\partial z} + \frac{\partial w}{\partial x} - C_1\frac{u}{R_x} - C_1\frac{v}{R_{xy}}, \quad \gamma_{yz} = \frac{\partial v}{\partial z} + \frac{\partial w}{\partial y} - C_1\frac{v}{R_y} - C_1\frac{u}{R_{xy}}, \end{aligned} \tag{2}$$

Substituting Eq. (1) in Eq. (2)

$$\begin{aligned} \varepsilon_x &= \varepsilon_{x0} + z\kappa_x + z^2\varepsilon_{x0}^* + z^3\kappa_x^* \\ \varepsilon_y &= \varepsilon_{y0} + z\kappa_y + z^2\varepsilon_{y0}^* + z^3\kappa_y^* \\ \gamma_{xy} &= \gamma_{xy0} + z\kappa_{xy} + z^2\gamma_{xy0}^* + z^3\kappa_{xy}^* \\ \gamma_{xz} &= \varphi_x + z\kappa_{xz} + z^2\varphi_x^* + z^3\kappa_{xz}^* \\ \gamma_{yz} &= \varphi_y + z\kappa_{yz} + z^2\varphi_y^* + z^3\kappa_{yz}^* \end{aligned} \tag{3}$$

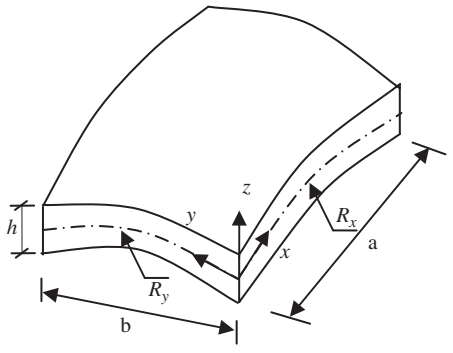

Fig. 1. FG spherical shell element.

where

$$\{\varepsilon_{x0}, \varepsilon_{y0}, \gamma_{xy0}, \varepsilon^*_{x0}, \varepsilon^*_{y0}, \gamma^*_{xy0}\} = \left\{\frac{\partial u_0}{\partial x} + \frac{w_0}{R_x}, \frac{\partial v_0}{\partial y} + \frac{w_0}{R_y}, \frac{\partial u_0}{\partial y} + \frac{\partial v_0}{\partial x} + \frac{2w_0}{R_{xy}}, \frac{\partial u^*_0}{\partial x}, \frac{\partial v^*_0}{\partial y}, \frac{\partial v^*_0}{\partial x} + \frac{\partial u^*_0}{\partial y}\right\}$$

$$\{\kappa_x, \kappa_y, \kappa_{xy}, \kappa^*_x, \kappa^*_y, \kappa^*_{xy}\} = \left\{\frac{\partial \theta_y}{\partial x}, -\frac{\partial \theta_x}{\partial y}, \frac{\partial \theta_y}{\partial y} - \frac{\partial \theta_x}{\partial x} + C_0\frac{\partial u_0}{\partial y} - C_0\frac{\partial v_0}{\partial x}, \frac{\partial \theta^*_y}{\partial x}, -\frac{\partial \theta^*_x}{\partial y}, \frac{\partial \theta^*_y}{\partial y} - \frac{\partial \theta^*_x}{\partial x}\right\}$$

$$\{\varphi_x, \varphi_y\} = \left\{\frac{\partial w_0}{\partial x} + \theta_y - C_1\frac{u_0}{R_x} - C_1\frac{v_0}{R_{xy}}, \frac{\partial w}{\partial y} - \theta_x - C_1\frac{v_0}{R_y} - C_1\frac{u_0}{R_{xy}}\right\}$$

$$\{\varphi^*_x, \varphi^*_y\} = \left\{3\theta^*_y - C_1\frac{u^*_0}{R_x} - C_1\frac{v^*_0}{R_{xy}}, -3\theta^*_x - C_1\frac{v^*_0}{R_y} - C_1\frac{u^*_0}{R_{xy}}\right\}$$

$$\{\kappa_{xz}, \kappa_{yz}, \kappa^*_{xz}, \kappa^*_{yz}\} = \left\{2u^*_o - C_1\frac{\theta_y}{R_x} + C_1\frac{\theta_x}{R_{xy}}, 2v^*_o + C_1\frac{\theta_x}{R_y} - C_1\frac{\theta_y}{R_{xy}}, -C_1\frac{\theta^*_y}{R_x} + C_1\frac{\theta^*_x}{R_{xy}}, C_1\frac{\theta^*_x}{R_x} - C_1\frac{\theta^*_y}{R_{xy}}\right\} \tag{4}$$

C_1 is a tracer by which the analysis can be reduced to that of shear deformable Love's first approximation and $C_0 = 0.5(1/R_x - 1/R_y)$ is the result of Sanders' theory which accounts for the condition of zero strain for rigid body motion.

3. FG material properties

The panels considered in the present analysis are assumed to be of uniform thickness h. Further, it is assumed that the panel is made from a mixture of ceramic and metals and the material composition is continuously varied such that the top surface ($z = h/2$) of the panel is ceramic rich, whereas the bottom surface ($z = -h/2$) is metal rich. Thus, the effective material property P (such as Young's modulus, Poisson's ratio, mass density, etc.) can be expressed as

$$P = \sum_{j=1}^{k} P_j V_j \tag{5}$$

where P_j and V_j are the material property and volume fraction of the constituent material j, satisfying the volume fraction of all the constituent materials k as

$$\sum_{j=1}^{k} V_j = 1 \tag{6}$$

For a panel with the reference surface at its middle surface, the volume fraction can be written as

$$V_j = \left(\frac{2z+h}{2h}\right)^n \tag{7}$$

in which, n characterizes the material variation through the panel thickness and $0 \leqslant n \leqslant \infty$.

Material properties for a FG solid with two constituent materials are given by

$$P(z) = (P_c - P_m)\left(\frac{2z+h}{2h}\right)^n + P_m \tag{8}$$

where P_c and P_m refer to the corresponding properties of the ceramic and metal constituents, respectively. By using these material properties, the stresses can be determined as

$$\begin{Bmatrix}\sigma_x\\ \sigma_y\\ \tau_{xy}\\ \tau_{yz}\\ \tau_{xz}\end{Bmatrix} = \begin{bmatrix}Q_{11} & Q_{12} & 0 & 0 & 0\\ Q_{12} & Q_{22} & 0 & 0 & 0\\ 0 & 0 & Q_{66} & 0 & 0\\ 0 & 0 & 0 & Q_{44} & 0\\ 0 & 0 & 0 & 0 & Q_{55}\end{bmatrix}\begin{Bmatrix}\varepsilon_x\\ \varepsilon_y\\ \gamma_{xy}\\ \gamma_{yz}\\ \gamma_{xz}\end{Bmatrix} \tag{9}$$

where

$$Q_{11} = Q_{22} = \frac{E(z)}{1-\nu(z)^2}, \quad Q_{12} = \frac{\nu(z)E(z)}{1-\nu(z)^2}, \quad Q_{44} = Q_{55} = Q_{66} = G(z) = \frac{E(z)}{2(1+\nu(z))} \tag{10}$$

Eq. (9) can also be written as

$$\boldsymbol{\sigma} = \overline{\mathbf{Q}}\boldsymbol{\varepsilon} \tag{11}$$

where $\overline{\mathbf{Q}}$ is the effective stiffness coefficient matrix given by the relation

$$\overline{\mathbf{Q}} = (\mathbf{Q}_c - \mathbf{Q}_m)\left(\frac{2z+h}{2h}\right)^n + \mathbf{Q}_m \tag{12}$$

$\mathbf{Q}_c$ and $\mathbf{Q}_m$ are the effective stiffness coefficient matrices for ceramic and metal constituents, respectively. Also, for the value of the power $n = 0$, the FG panel becomes ceramic rich and metal rich for the value $n = \infty$.

Integrating the stresses through the thickness, the resultant forces and moments acting on the panel are obtained.

$$\begin{bmatrix} N_x & N_x^* \\ N_y & N_y^* \\ N_{xy} & N_{xy}^* \end{bmatrix} = \int_{-h/2}^{h/2} \begin{bmatrix} \sigma_x \\ \sigma_y \\ \tau_{xy} \end{bmatrix} [1, z^2]\,\mathrm{d}z$$

$$\begin{bmatrix} M_x & M_x^* \\ M_y & M_y^* \\ M_{xy} & M_{xy}^* \end{bmatrix} = \int_{-h/2}^{h/2} \begin{bmatrix} \sigma_x \\ \sigma_y \\ \tau_{xy} \end{bmatrix} [z, z^3]\,\mathrm{d}z$$

$$\begin{bmatrix} P_x & S_x & P_x^* & S_x^* \\ P_y & S_y & P_y^* & S_y^* \end{bmatrix} = \int_{-h/2}^{h/2} \begin{bmatrix} \tau_{xz} \\ \tau_{yz} \end{bmatrix} [1, z, z^2, z^3]\,\mathrm{d}z \tag{13}$$

or $\overline{\boldsymbol{\sigma}} = \mathbf{D}\overline{\boldsymbol{\varepsilon}}$, where

$$\overline{\boldsymbol{\sigma}} = (N_x, N_y, N_{xy}, N_x^*, N_y^*, N_{xy}^*, M_x, M_y, M_{xy}, M_x^*, M_y^*, M_{xy}^*, P_x, P_y, P_x^*, P_y^*, S_x, S_y, S_x^*, S_y^*)^{\mathrm{T}}$$

$$\overline{\boldsymbol{\varepsilon}} = (\varepsilon_{x0}, \varepsilon_{y0}, \gamma_{xy0}, \varepsilon_{x0}^*, \varepsilon_{y0}^*, \gamma_{xy0}^*, \kappa_x, \kappa_y, \kappa_{xy}, \kappa_x^*, \kappa_y^*, \kappa_{xy}^*, \varphi_x, \varphi_y, \varphi_x^*, \varphi_y^*, \kappa_{xz}, \kappa_{yz}, \kappa_{xz}^*, \kappa_{yz}^*)^{\mathrm{T}}$$

$$\mathbf{D} = \begin{bmatrix} \mathbf{D}_m & \mathbf{D}_c & 0 \\ \mathbf{D}_c^{\mathrm{T}} & \mathbf{D}_b & 0 \\ 0 & 0 & \mathbf{D}_s \end{bmatrix},$$

where $\mathbf{D}_m$, $\mathbf{D}_b$, $\mathbf{D}_c$ and $\mathbf{D}_s$ are written in the following terms:

$$\mathbf{D}_m = \begin{bmatrix} \mathbf{H}_1 & \mathbf{H}_3 \\ \mathbf{H}_3 & \mathbf{H}_5 \end{bmatrix}$$

The elements of $\mathbf{D}_c$ and $\mathbf{D}_b$ matrices can be obtained by replacing ($\mathbf{H}_1$, $\mathbf{H}_3$ and $\mathbf{H}_5$) by ($\mathbf{H}_2$, $\mathbf{H}_4$ and $\mathbf{H}_6$) and ($\mathbf{H}_3$, $\mathbf{H}_5$ and $\mathbf{H}_7$), respectively, and

$$(\mathbf{H}_1, \mathbf{H}_2, \mathbf{H}_3, \mathbf{H}_4, \mathbf{H}_5, \mathbf{H}_6, \mathbf{H}_7) = \int_{-h/2}^{h/2} \overline{\mathbf{Q}}_{ij}(1, z, z^2, z^3, z^4, z^5, z^6)\,\mathrm{d}z, \quad i,j = 1,2,6$$

$$D_s = \begin{bmatrix} \overline{\mathbf{H}}_1 & \overline{\mathbf{H}}_3 & \overline{\mathbf{H}}_2 & \overline{\mathbf{H}}_4 \\ & \overline{\mathbf{H}}_5 & \overline{\mathbf{H}}_4 & \overline{\mathbf{H}}_6 \\ & \text{sym} & \overline{\mathbf{H}}_3 & \overline{\mathbf{H}}_5 \\ & & & \overline{\mathbf{H}}_7 \end{bmatrix}$$

in which

$$(\overline{\mathbf{H}}_1, \overline{\mathbf{H}}_2, \overline{\mathbf{H}}_3, \overline{\mathbf{H}}_4, \overline{\mathbf{H}}_5, \overline{\mathbf{H}}_6, \overline{\mathbf{H}}_7) = \int_{-h/2}^{h/2} \overline{\mathbf{Q}}_{ij}(1, z, z^2, z^3, z^4, z^5, z^6)\,\mathrm{d}z, \quad i,j = 1,4,5$$

where $\overline{\mathbf{Q}}$ is given in Eq. (12).

4. Finite element formulation

In the present study, an eight-noded C^o element with nine degrees of freedom is considered. The displacement vector at any point on the mid-surface is given by

$$\Delta = \sum_{i=1}^{8} N_i \Delta_i \tag{14}$$

in which $\Delta = (u_0, v_0, w_0, \theta_x, \theta_y, u_0^*, v_0^*, \theta_x^*, \theta_y^*)^{\mathrm{T}}$ at any point (x, y) in the mid-surface, and Δ_i is the displacement vector corresponding to node i and N_i is the interpolating function associated with the node i, given by

$$\begin{aligned} N_i &= (1+\xi\xi_i)(1+\eta\eta_i)(\xi\xi_i+\eta\eta_i-1)/4, && i = 1 \text{ to } 4 \\ N_i &= (1-x_2)(1+\xi\xi_i)/2, && i = 5,\ 7 \\ N_i &= (1+\xi\xi_i)(1-\eta^2)/2, && i = 6,\ 8 \end{aligned} \tag{15}$$

where ξ_i and η_i are the coordinates ξ and η of the mid-surface.

The strain–displacement relationship is expressed in the matrix form as

$$\overline{\boldsymbol{\varepsilon}} = \mathbf{B}\mathbf{d} \tag{16}$$

where $\mathbf{B}$ is a differential operator matrix of interpolation functions which can be obtained from Eq. (4) and $\mathbf{d} = \{\boldsymbol{\Delta}_1 \cdots \boldsymbol{\Delta}_8\}^{\mathrm{T}}$ is the element displacement vector.

The governing differential equations of motion according to Hamilton's principle is given as [34]

$$\delta \int_{t_1}^{t_2} \left(\prod - T \right) \mathrm{d}t = 0 \tag{17}$$

where t is the time, T the total kinetic energy of the system and Π the potential energy of the system including both strain energy and potential conservative external forces. For the ideal case in which the system has no damping and no external forcing function, the mathematical statement of Hamilton's principle can be written as

$$\int_{t_1}^{t_2} (\delta U - \delta T)\,\mathrm{d}t = 0 \tag{18}$$

where δU and δT are the first variation of the strain energy and the kinetic energy, respectively.

The first variation of δU and δT can be written in matrix form as

$$\delta U = \delta \mathbf{d}^{\mathbf{t}} \mathbf{K} \mathbf{d} \quad \text{and} \quad \delta T = -\delta \mathbf{d}^{\mathbf{t}} \mathbf{M} \mathbf{d} \tag{19}$$

in which $\mathbf{K}$ and $\mathbf{M}$ are the global stiffness and mass matrices, which are obtained by assembling the corresponding element matrices. For any element e, the element stiffness and mass matrices $\mathbf{K}_e$ and $\mathbf{M}_e$ are

evaluated by

$$\mathbf{K}_e = \int_A \mathbf{B}^{\mathbf{T}}\mathbf{D}\mathbf{B}\,\mathrm{d}A \quad \text{and} \quad \mathbf{M}_e = \int_A \mathbf{N}^{\mathbf{T}}\mathbf{m}\mathbf{N}\,\mathrm{d}A \tag{20}$$

where $\mathbf{N}$ is the shape function matrix and $\mathbf{m}$ the inertia matrix, as given in Appendix A. In all the numerical computations, the selective integration rule is employed. A 3×3 Gaussian rule is used to compute in-plane, coupling between in-plane and bending deformations; while a 2×2 integration rule is used to evaluate the terms associated with transverse shear deformation. The free vibration analysis involves determination of natural frequencies from the condition

$$(\mathbf{K} - \omega^2\mathbf{M}) = 0 \tag{21}$$

This is a generalized eigenvalue problem and is solved using subspace iteration method to get the natural frequency ω.

5. Boundary conditions

The following two boundary conditions are used in the present analysis:

(i) Simply supported boundary: $v_0 = w_0 = \theta_y = v_0^* = \theta_y^* = 0$ at $x = 0$, a and $u_0 = w_0 = \theta_x = u_0^* = \theta_x^* = 0$ at $y = 0$, b.
(ii) Clamped boundary: $u_0 = v_0 = w_0 = \theta_x = \theta_y = u_0^* = v_0^* = \theta_x^* = \theta_y^* = 0$ at $x = 0$, a and $y = 0$, b.

6. Convergence and comparison problems

Unless specified, the material properties for the convergence and comparison problems are considered as, for aluminum: $E_m = 70\,\mathrm{GPa}$, $\nu_m = 0.3$ and $\rho_m = 2707\,\mathrm{kg/m^3}$ and for zirconia: $E_c = 200\,\mathrm{GPa}$, $\nu_c = 0.3$ and $\rho_c = 2702\,\mathrm{kg/m^3}$ and the obtained natural frequencies are non-dimensionalized as $\omega^* = \omega h^2\sqrt{\rho_m/E_m}$.

6.1. Convergence study

Convergence study is carried out in order to determine the uniform mesh size at which the natural frequencies converge. Table 1 shows the convergence results of a simply supported aluminum–zirconia square FG plate. From Table 1, it is found that the non-dimensional frequencies ω^* converge for the uniform mesh size of 8×8. Therefore, the subsequent investigations are carried out using the uniform mesh size of 8×8.

Table 1
Convergence of non-dimensional frequency parameter of simply supported aluminum–zirconia FG plate $a/b = 1$, $\omega^* = \omega h^2\sqrt{\rho_m/E_m}$

Mesh size	$n = 1$			$a/h = 5$			$n = 0$	
	$a/h = 5$	$a/h = 10$	$a/h = 20$	$n = 2$	$n = 3$	$n = 5$	$a/h = \sqrt{10}$	$a/h = 10$
4×4	0.2253	0.0612	0.0157	0.2233	0.2239	0.2249	0.4582	0.0577
6×6	0.2256	0.0613	0.0157	0.2236	0.2242	0.2252	0.4657	0.0577
8×8	0.2257	0.0613	0.0157	0.2237	0.2243	0.2253	0.4658	0.0578
10×10	0.2257	0.0613	0.0157	0.2237	0.2243	0.2253	0.4658	0.0578
12×12	0.2257	0.0613	0.0157	0.2237	0.2244	0.2253	0.4658	0.0578

Table 2
Comparison of non-dimensional frequency parameter $\omega^* = \omega h^2\sqrt{\rho_m/E_m}$ for a simply supported aluminum–zirconia plate

Results	$n=1$			$a/h=5$			$n=0$	
	$a/h=5$	$a/h=10$	$a/h=20$	$n=2$	$n=3$	$n=5$	$a/h=\sqrt{10}$	$a/h=10$
Present HSDT	0.2257	0.0613	0.0157	0.2237	0.2243	0.2253	0.4658	0.0578
FSDT	0.2323	0.0633	0.0162	0.2325	0.2334	0.2334	0.4619	0.0577
3-D [35]	0.2192	0.0596	0.0153	0.2197	0.2211	0.2225	0.4658 (0.5535[a])	0.0578 (0.0592[a])
HSDT [36]	0.2285	0.0618	0.0158	0.2264	0.227	0.2281	0.4658	0.0578
Ref. [37]	0.2188	0.0592	0.0147	0.2153	0.2202	0.2215	–	–
Ref. [38]	0.2188	0.0584	0.0149	0.2153	0.2172	0.2194	–	–

[a]Results of CPT.

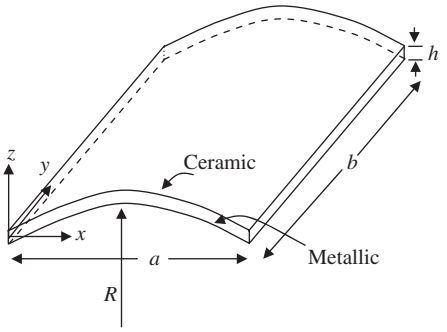

Fig. 2. FG cylindrical shell panel.

6.2. Comparison studies

In order to establish the correctness of the present formulation, the following examples are considered and the obtained results are compared with those existing in the literature.

1. Natural frequencies of simply supported square aluminum–zirconia FG plate are obtained using the present HSDT and the first-order shear deformation theory (FSDT) considering a shear correction factor of 5/6. The obtained results are compared with those of 3-D exact solutions of Vel and Batra [35], 2-D higher-order theory solutions of Matsunaga [36] and meshless method solutions of Ferreira et al. [37] and Qian et al. [38] in Table 2. From Table 2, it is observed that, for plates with $n=0$, i.e. for pure ceramic plates, the present HSDT results of ω^* are in excellent agreement with those of Vel and Batra [35] and Matsunaga [36]. Classical plate theory (CPT) solutions of ω^* obtained by Vel and Batra [35] are also given in Table 2 for pure ceramic plate ($n=0$) with $a/h=\sqrt{10}$ and 10. It is seen from Table 2 that the difference between the corresponding CPT and the HSDT/3-D results, for pure ceramic plates, increases from 2.4% to 18.8% when the a/h ratio is decreased from 10 to $\sqrt{10}$. It is also observed that for $a/h=\sqrt{10}$, the CPT overpredicts the natural frequencies. Since the effect of transverse shear deformation is neglected in CPT, the above behavior is obvious for thick plates (for $a/h<10$). Similar behavior was observed by Ng et al. [39] in their prediction of origin of dynamic stability of isotropic cylindrical shell panels. It was observed in Ref. [39] that the inclusion of transverse shear stresses and rotary inertia effects in the first and higher-order theories generate more conservative results. For FG plates with higher values of n (for $n>0$), the present HSDT results are on the higher side than the corresponding 3-D results of Ref. [35] and meshless solutions of Refs. [37,38]. However, the authors' results are in between the 3-D results of Vel and Batra [35] and 2-D higher-order results of Matsunaga [36]. The differences between the results of Refs. [35,37,38] and HSDT results of authors and Matsunaga [36] are due to the different scheme of homogenization of material properties adopted. Investigators in Refs. [35,37,38] adopted Mori–Tanaka scheme of homogenization, whereas, Voigt rule of mixtures was used by the authors and Matsunaga [36].

Table 3
Comparison of non-dimensional frequency parameter $\omega^* = \omega a^2\sqrt{\rho_m h/D_m^*}$ for a clamped FG cylindrical shell panel

Mode	Material composition	Si_3N_4	$n = 0.2$	$n = 2.0$	$n = 10.0$	SUS304
1	Present HSDT	72.9613	60.0269	39.1457	33.3666	32.0274
	Ref. [18]	74.518	57.479	40.750	35.852	32.761
2	Present HSDT	138.5552	113.8806	74.2915	63.2869	60.5546
	Ref. [18]	144.663	111.717	78.817	69.075	63.314
3	Present HSDT	138.5552	114.0266	74.3868	63.3668	60.6302
	Ref. [18]	145.740	112.531	79.407	69.609	63.806
4	Present HSDT	195.5366	160.6235	104.7687	89.1970	85.1788
	Ref. [18]	206.992	159.855	112.457	98.386	90.370

Table 4
Comparison of performance of HSDT and FSDT for aluminum–alumina plate for different a/h values $\omega^* = \omega a^2\sqrt{\rho_m h/D_m^*}$, $D_m^* = E_m h^3/(12(1-\nu_m^2))$

a/h	$n = 0.0$		$n = 0.5$		$n = 1.0$	
	HSDT	FSDT	HSDT	FSDT	HSDT	FSDT
5	58.2858	56.5548	48.7185	47.2468	43.4243	42.0305
10	71.7395	70.8035	58.5305	57.7597	52.0173	51.0884
15	75.0439	75.7838	61.5835	62.2838	54.7015	55.4209
20	77.0246	77.5654	63.1381	63.8393	56.0880	56.7991
50	84.8800	85.4346	69.8604	70.3199	62.2152	62.8458
100	102.9227	103.4855	86.5452	87.1049	77.0774	77.7762

2. A FG cylindrical panel (Fig. 2) having clamped boundaries is considered with geometric properties $a/h = 10$, $a/R = 0.1$, $a = b$ and with different values of n from 0 to ∞. The constituents of the FGM panel considered in this example are silicon nitride (Si_3N_4) and stainless steel (SUS304), whose material properties are given below:

   Si_3N_4 (ceramic): $E_c = 322.2715\,\text{GPa}$, $\nu_c = 0.24$, $\rho_c = 2370\,\text{kg/m}^3$ and
   SUS304 (metal): $E_m = 207.7877\,\text{GPa}$, $\nu_m = 0.31776$, $\rho_m = 8166\,\text{kg/m}^3$.

Non-dimensional frequency parameter is $\omega^* = \omega a^2\sqrt{\rho_m h/D_m^*}$ in which $D_m^* = E_m h^3/12(1-\nu_m^2)$.

Free vibration analysis of a clamped FG cylindrical shell panel is carried out using the present formulation. The values of first four non-dimensional frequencies are presented in Table 3 for different values of volume fraction index n along with those of Yang and Shen [18]. From Table 3, it is observed that there is a discrepancy between the authors' HSDT results and those of Yang and Shen [18]. The different higher-order theory (Reddy's higher-order shear deformation shell theory) and method of analysis (semi-analytical approach using one-dimensional (1-D) differential quadrature approximation and Galerkin technique) adopted by the earlier investigators in Ref. [18] may be the possible reasons for the deviation in the values of natural frequencies. It may be noted that ω^* is the maximum for pure ceramic and gradually reduces for the composite with the increase of n and becomes the minimum for pure metallic FG clamped cylindrical panel.

The validation of authors' results establishes the use of present formulation for calculating the ω^* of different FG plates and shells of different compositions.

6.3. Performance of the present HSDT

Before taking up additional problems to investigate the effect of different parameters on the natural frequency of different shell forms made up of FG panels, the performance of the present HSDT is compared with that of the FSDT. Constituents of the FGM used in the subsequent analysis are aluminum (metal) and

alumina (ceramic) whose material properties are, for Aluminum, $E_m = 70\,\text{GPa}$, $\nu_m = 0.3$, $\rho_m = 2707\,\text{kg/m}^3$and for Alumina, $E_c = 380\,\text{GPa}$, $\nu_c = 0.3$, $\rho_c = 3000\,\text{kg/m}^3$. Non-dimensional frequency parameter $\omega^* = \omega a^2\sqrt{\rho_m h/D_m^*}$ in which $D_m^* = E_m h^3/(12(1-\nu_m^2))$. The non-dimensional frequency parameters of cylindrical FG panels made up of aluminum and alumina with different a/h ratios using the present HSDT and the FSDT are tabulated in Table 4. From Table 4, it is found that for thick panels (panels having $a/h \leqslant 10$), the FSDT, based on Mindlin's approximations, underpredicts the natural frequencies than the corresponding HSDT ones. On the other hand for thin panels, FSDT overpredicts the values of non-dimensional frequency parameters compared with the same using HSDT. From the above observation, it is inferred that the present HSDT formulation, though computationally expensive, shows good performance for both thin as well as thick panels and hence recommended for free vibration analysis of both thin and thick FG plates and shell panels.

7. Additional problems

The authors' HSDT formulation has been used for the three additional problems to include cylindrical ($R = R_x$, $R_y = R_{xy} = \infty$, Fig. 2), spherical ($R_x = R_y = R, R_{xy} = \infty$, Fig. 1) and hypar ($R_x = R_y = \infty$, Fig. 3) shell panels. The FG panels considered in these investigations are made up of aluminum and alumina and the properties of the same and the non-dimensional frequency parameter are taken from the previous investigation. For all the three problems, both clamped and simply supported boundary conditions are used and the volume fraction index n is varied from 0 to ∞.

The following are the parametric variations of the three problems taken up in the present study:

1. The parameters R/a and a/h are varied from 0.5 to $\infty$and 10 to 100, respectively, for the cylindrical and spherical shell panels.
2. The parameter c/a is varied from 0 to 0.2 for the hypar shell panel.

The numerical results of the three problems are presented in tables and figures as mentioned below:

1. Tables 5 and 6 present results of ω^* of the cylindrical shell panel having simply supported and clamped boundary conditions, respectively, with the variations of R/a and n.

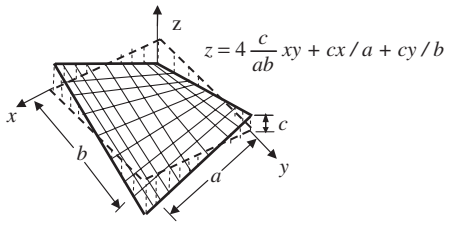

Fig. 3. Hypar shell.

Table 5
Non-dimensional frequency parameter $\omega^* = \omega a^2\sqrt{\rho_m h/D_m^*}$ for simply supported cylindrical FG shell panels with different R/a ratios

$R/a \rightarrow n$	0.5	1.0	5	10	50	Plate
0	68.8645	51.5216	42.2543	41.9080	41.7963	41.7917
0.2	64.4001	47.5968	40.1621	39.8472	39.7465	39.7426
0.5	59.4396	43.3019	37.2870	36.9995	36.9088	36.9057
1.0	53.9296	38.7715	33.2268	32.9585	32.8750	32.8726
2.0	47.8259	34.3338	27.4449	27.1789	27.0961	27.0937
10.0	37.2593	28.2757	19.3892	19.1562	19.0809	19.0778
∞	31.9866	24.1988	19.0917	18.9352	18.8848	18.8827

Table 6
Non-dimensional frequency parameter $\omega^* = \omega a^2\sqrt{\rho_m h/D_m^*}$ for clamped cylindrical FG shell panels with different R/a ratios

$R/a \rightarrow n$	0.5	1	5	10	50	Plate
0	129.9808	94.4973	71.8861	71.0394	70.766	70.7546
0.2	119.6109	87.3930	68.1152	67.3320	67.0801	67.0698
0.5	108.1546	79.5689	63.1896	62.4687	62.2380	62.2291
1.0	96.0666	71.2453	56.5546	55.8911	55.6799	55.6722
2.0	84.4431	62.9748	36.2487	35.6633	35.4745	35.4669
10.0	69.8224	51.3803	33.6611	33.1474	32.9812	32.9743
∞	61.0568	44.2962	32.4802	32.0976	31.9741	31.9689

Table 7
Non-dimensional frequency parameter $\omega^* = \omega a^2\sqrt{\rho_m h/D_m^*}$ for simply supported spherical FG shell panels with different R/a ratios

$R/a \rightarrow n$	0.5	1	5	10	50	Plate
0	124.1581	78.2306	44.0073	42.3579	41.8145	41.7917
0.2	115.7499	72.6343	41.7782	40.2608	39.7629	39.7426
0.5	106.5014	66.5025	38.7731	37.3785	36.9234	36.9057
1.0	96.2587	59.8521	34.6004	33.3080	32.8881	32.8726
2.0	84.8206	52.7875	28.7459	27.5110	27.1085	27.0937
10.0	65.2296	41.6702	20.4691	19.4357	19.0922	19.0778
∞	57.2005	36.2904	19.8838	19.1385	18.8930	18.8827

Table 8
Non-dimensional frequency parameter $\omega^* = \omega a^2\sqrt{\rho_m h/D_m^*}$ for clamped spherical FG shell panels with different R/a ratios

$R/a \rightarrow n$	0.5	1	5	10	50	Plate
0	173.9595	120.9210	73.5550	71.4659	70.7832	70.7546
0.2	161.3704	112.2017	69.6597	67.7257	67.0956	67.0698
0.5	147.4598	102.5983	64.6114	62.8299	62.2519	62.2291
1.0	132.3396	92.2147	57.8619	56.2222	55.6923	55.6722
2.0	116.4386	81.3963	37.3914	35.9568	35.4861	35.4669
10.0	92.1387	64.8773	34.6658	33.4057	32.9916	32.9743
∞	80.7722	56.2999	33.2343	32.2904	31.9819	31.9689

2. Tables 7 and 8 present results of ω^* of the spherical shell panel having simply supported and clamped boundary conditions, respectively, with the variations of R/a and n.
3. Figs. 4 and 5 show the variations of ω^* for different values of a/h and n of FG cylindrical shell panels with simply supported and clamped boundary conditions, respectively.
4. Figs. 6 and 7 show the variations of ω^* for different values of a/h and n of FG spherical shell panels with simply supported and clamped boundary conditions, respectively.
5. Figs. 8 and 9 present results of ω^* of the hypar shell panel having simply supported and clamped boundary conditions, respectively, with the variations of c/a and n.

A detailed study of the results of Tables 5–8 and Figs. 4–9 reveal the following.

1. The values of ω^* for clamped boundary conditions are much higher (about 1.5–2 times) than those having simply supported boundaries.
2. The values of ω^* are consistently increasing with the (i) decrease of R/a for any constant value of n and (ii) decrease of n for any constant value of R/a as seen from Tables 5–8.

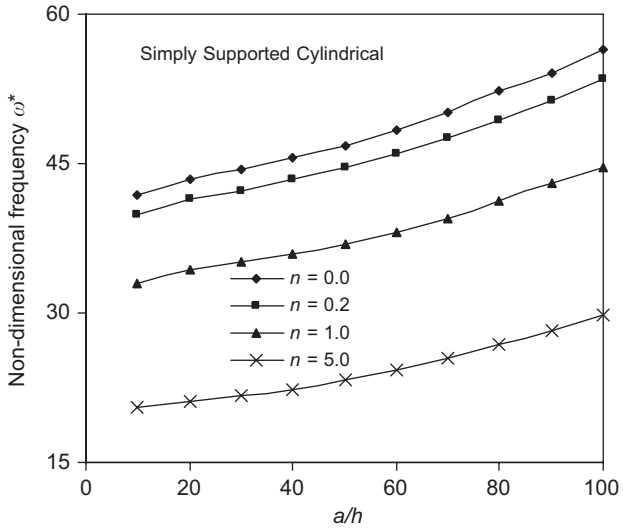

Fig. 4. Effect of a/h ratio on the non-dimensional frequency parameter ω^* of a simply supported cylindrical FG shell panel.

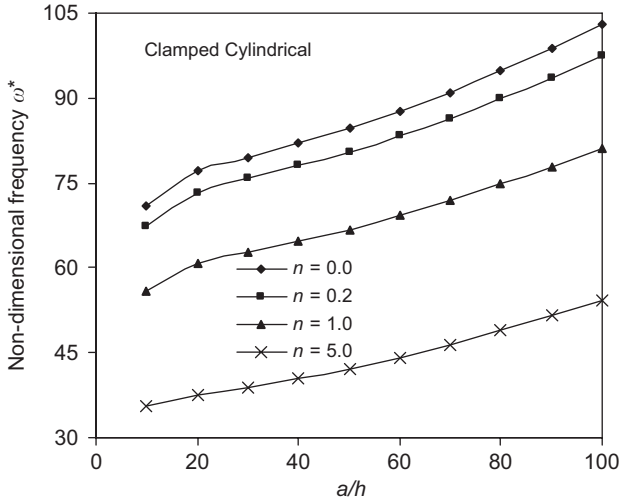

Fig. 5. Effect of a/h ratio on the non-dimensional frequency parameter ω^* of a clamped cylindrical FG shell panel.

The two observations can be justified by the two interactive effects of stiffness K and mass M in determining the frequency parameters. The first observation shows the superiority of shells with lower values of R/a where the increase of ω^* is mostly due to the increase of stiffness of shells than that of plates. The second observation establishes the superiority of pure ceramic to other composites. It may be noted that ceramic is heavier than the metal of this problem. The heavier mass of ceramic should have reduced the frequency ω^*. Therefore, the increased value of ω^*, in spite of the heavier mass of ceramic, shows the dominance of stiffness effect K rather than the mass M. Thus, both the observations reveal the dominance of the stiffness in increasing the values of ω^* for this problem.

It is worth mentioning that the results of Table 3 (comparative problem 2), exhibiting increase of ω^* with lower value of n, i.e. for ceramic, which is lighter than the metal, show that both mass M and stiffness K are contributing factors in increasing the value of ω^*.

3. The results of Figs. 4–7 show the increasing trend of ω^* with the (i) increase of a/h ratios or the decrease of the thickness h for fixed values of a and n (ii) decrease of n for fixed values of a/h. Here also, the increasing

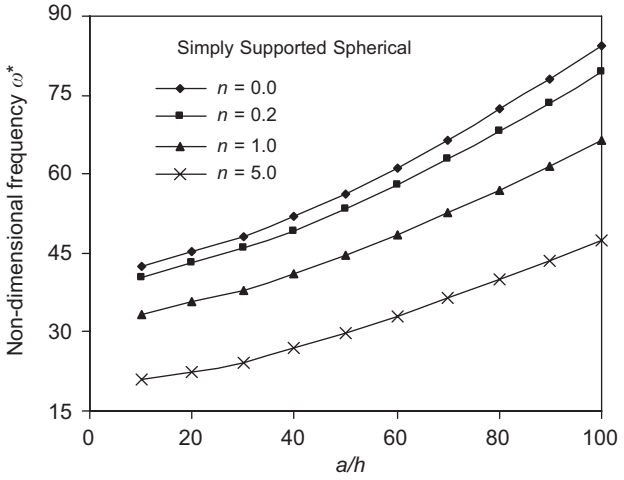

Fig. 6. Effect of a/h ratio on the non-dimensional frequency parameter ω^* of a simply supported spherical FG shell panel.

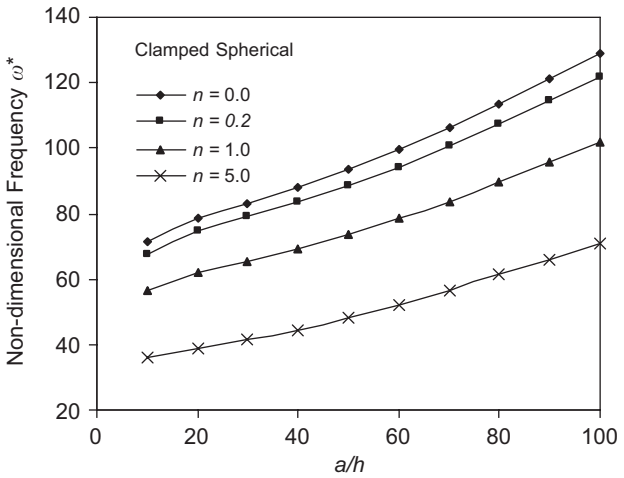

Fig. 7. Effect of a/h ratio on the non-dimensional frequency parameter ω^* of a clamped spherical FG shell panel.

trend of ω^* for increasing/decreasing values of a/h or n can be explained by the respective dominance of effect of mass and stiffness as explained in Eq. (2) above. However, it is important to note that the decrease of n shows the effect of stiffness both for the constant values of R/a (Tables 5–8) and a/h (Figs. 4–7).

4. Results of Figs. 8 and 9 also confirm the effect of stiffness in increasing the ω^* when n is reduced from metal to ceramic. The increasing trend of ω^* with the increase of c/a is, however, very stiff initially up to $c/a = 0.05$ and then relatively lower for further increase of c/a as seen from Fig. 8 for the simply supported hypar shell. For the clamped hypar shells, the increasing trend of ω^* is almost uniform with the increase of c/a, establishes the superiority of clamped hypar shells once again. Here again, the relative increase of ω^* with the change of n or c/a as discussed above may be explained with the respective influence of the effect of the mass or the stiffness for the particular case.

Table 9 presents the maximum and minimum values of ω^* corresponding to $n = 0$ and ∞ of three different shell panels viz. (i) singly curved cylindrical, (ii) doubly curved synclastic spherical and (iii) doubly curved anticlastic hypar panels having the same or equivalent geometric parameters of $R/a = 5$ and 10 and equivalent $c/a = 0.2$ and 0.1 for both simply supported and clamped boundary conditions.

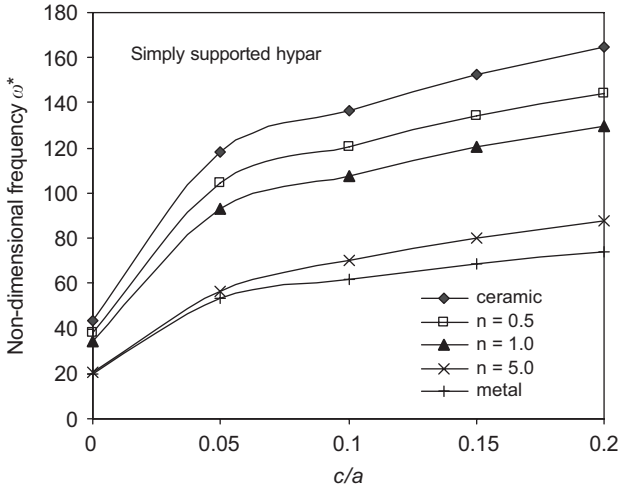

Fig. 8. Non-dimensional frequency parameter ω^* of a simply supported hypar shell for different c/a ratios.

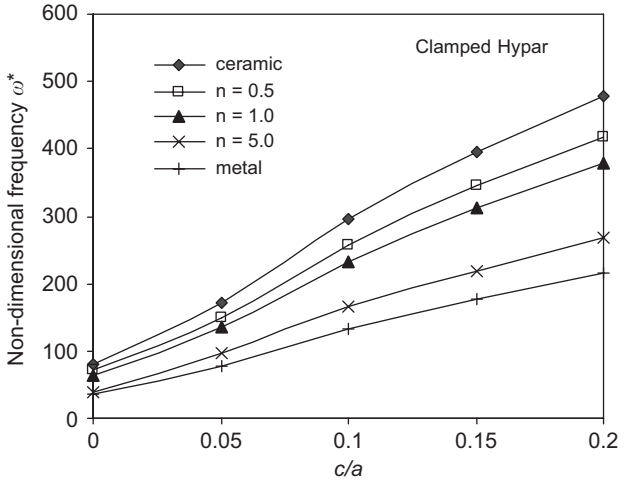

Fig. 9. Non-dimensional frequency parameter ω^* of a clamped hypar shell for different c/a ratios.

Table 9
Range of values of ω^* corresponding to $n = 0$ and ∞ of different shell forms

Shell form	Simply supported		Clamped	
	$R/a = 5$, $c/a = 0.2$	$R/a = 10$, $c/a = 0.1$	$R/a = 5$, $c/a = 0.2$	$R/a = 10$, $c/a = 0.1$
Cylindrical	19.09–42.25	18.94–41.91	32.48–71.89	32.1–71.04
Spherical	19.88–44.01	19.14–42.36	33.23–73.56	32.29–71.47
Hypar	74.33–164.52	61.75–136.68	216.65–479.5	133.54–295.55

The comparison of the values of ω^* from Table 9 gives the order of superiority of the three shell forms considering ω^* as the sole criterion. A study of the value ω^* clearly shows the best performance of the anticlastic hypar shells. Though the values of ω^* for spherical and cylindrical are more or less in the same ranges, the doubly curved spherical shell proves itself to be marginally better than the singly curved cylindrical panels. The above order of superiority of the shell panels are for both types of the boundary conditions, i.e. simply supported and clamped and for each of the material compositions for the same or equivalent values

of the curvature parameters. It may, therefore, be inferred that the three shell panels may be arranged as hypar, spherical and cylindrical shell panels in descending order of their respective values of ω^*.

8. Conclusions

The following conclusions are derived:

A. The authors' HSDT formulations may be recommended for determining the values of ω^* of plate and shell panels. This is based on observing good agreement between the authors' results with those available in the published literature.
B. Comparative study of values of ω^* of three additional shell panels leads to the following conclusions.
   1. As expected, the clamped boundary condition is a better performer showing higher values of ω^* for all the three types of shell panels and for different values of other geometric parameters.
   2. Both for the cylindrical and spherical shells, the gradual decrease of the values of R improves the values of ω^* when the other geometrical parameters, boundary conditions and volume fraction index n are kept constants.
   3. For hypar shells, the increasing value of c improves the value of ω^* for identical geometrical parameters, boundary conditions and volume fraction index n.
   4. Both for the cylindrical and spherical shells, decrease of the thickness h improves ω^* when other geometrical properties, boundary conditions and volume fraction index n are kept constants.
   5. The increase of ω^* of shell panels either due to decrease of radius parameter R/a or increase of thickness parameter a/h is possibly due to the dominance of either the stiffness or mass effect in the respective cases.
   6. Comparative study of the values of ω^* for the same or identical values of radius parameter establishes the superiority of the hypar shell followed by the spherical and the cylindrical shell panels irrespective of the boundary conditions and the volume fraction index n.

Acknowledgments

The authors are thankful to the AICTE, New Delhi, for providing financial assistance to carry out this research work under the National Doctoral Fellowship Scheme.

Appendix A

The inertia matrix [**m**] for the present higher-order theory is given by

$$\mathbf{m} = \begin{bmatrix} I_1 & 0 & 0 & 0 & I_2 & I_3 & 0 & 0 & I_4 \\ 0 & I_1 & 0 & -I_2 & 0 & 0 & I_3 & -I_4 & 0 \\ 0 & 0 & I_1 & 0 & 0 & 0 & 0 & 0 & 0 \\ 0 & -I_2 & 0 & I_3 & 0 & 0 & -I_4 & I_5 & 0 \\ I_2 & 0 & 0 & 0 & I_3 & I_4 & 0 & 0 & I_5 \\ I_3 & 0 & 0 & 0 & I_4 & I_5 & 0 & 0 & I_6 \\ 0 & I_3 & 0 & -I_4 & 0 & 0 & I_5 & -I_6 & 0 \\ 0 & -I_4 & 0 & I_5 & 0 & 0 & -I_6 & I_7 & 0 \\ I_4 & 0 & 0 & 0 & I_5 & I_6 & 0 & 0 & I_7 \end{bmatrix}$$

The parameters I_1, I_3 and (I_5, I_7) are linear inertia, rotary inertia and higher-order inertia terms, respectively. The parameters I_2, I_4 and I_6 are the coupling inertia terms and are expressed as follows:

$$(I_1, I_2, I_3, I_4, I_5, I_6, I_7) = \int_{-h/2}^{h/2} (1, z, z^2, z^3, z^4, z^5, z^6)\overline{\rho}\,\mathrm{d}z,$$

where $\overline{\rho} = (\rho_c - \rho_m)\left[(2z+h)/2h\right]^n + \rho_m$ and the shape function matrix [**N**] is given by

$$\mathbf{N} = \begin{bmatrix} N_i & & & & & & & \\ & N_i & & & & & & \\ & & N_i & & & & & \\ & & & N_i & & & & \\ & & & & N_i & & & \\ & & & & & N_i & & \\ & & & & & & N_i & \\ & & & & & & & N_i \end{bmatrix}$$

$i = 1, 8$ and N_i is the shape function for the node i.

References

[1] Y. Fukui, N. Yamanaka, Elastic analysis for thick-walled tubes of functionally graded material subjected to internal pressure, *JSME International Journal, Series 1: Solid Mechanics, Strength of Materials* 35 (1992) 379.

[2] V. Birman, Buckling of functionally graded hybrid composite plates, *Proceedings of the 10th Conference on Engineering Mechanics*, Boulder, USA, 1995.

[3] J. Aboudi, M.J. Pindera, S.M. Arnold, Higher-order theory for functionally graded materials, *Composites Part B: Engineering* 30 (1999) 777–832.

[4] J.N. Reddy, Analysis of functionally graded plates, *International Journal for Numerical Methods in Engineering* 47 (2000) 663–684.

[5] B.V. Sankar, An elasticity solution for functionally graded beams, *Composite Science and Technology* 61 (2001) 689–696.

[6] J. Woo, S.A. Meguid, Nonlinear analysis of functionally graded plates and shallow shells, *International Journal of Solids and Structures* 38 (2001) 7409–7421.

[7] A. Chakraborty, S. Gopalakrishnan, J.N. Reddy, A new beam finite element for the analysis of functionally graded materials, *International Journal of Mechanical Sciences* 45 (2003) 519–539.

[8] L.D. Croce, P. Venini, Finite elements for functionally graded Reissner–Mindlin plates, *Computer Methods in Applied Mechanics and Engineering* 193 (2004) 705–725.

[9] R.K. Bhangale, N. Ganesan, Static analysis of simply supported functionally graded and layered magneto-electro-elastic plates, *International Journal of Solids and Structures* 43 (2006) 3230–3253.

[10] H.-S. Shen, Nonlinear bending response of functionally graded plates subjected to transverse loads and in thermal environments, *International Journal of Mechanical Sciences* 44 (2002) 561–584.

[11] S.A.M. Ghannad Pour, M.M. Alinia, Large deflection behavior of functionally graded plates under pressure loads, *Composite Structures* 75 (2006) 67–71.

[12] G.N. Praveen, J.N. Reddy, Nonlinear transient thermoelastic analysis of functionally graded ceramic-metal plates, *International Journal of Solids and Structures* 35 (1998) 4457–4476.

[13] C.T. Loy, K.Y. Lam, J.N. Reddy, Vibration of functionally graded cylindrical shells, *International Journal of Solids and Structures* 41 (1999) 309–324.

[14] S.C. Pradhan, C.T. Loy, K.Y. Lam, J.N. Reddy, Vibration characteristics of functionally graded cylindrical shells under various boundary conditions, *Applied Accoustics* 61 (2000) 111–129.

[15] T.Y. Ng, K.Y. Lam, K.M. Liew, Effects of FGM materials on the parametric resonance of plate structures, *Computer Methods in Applied Mechanics and Engineering* 190 (2000) 953–962.

[16] T.Y. Ng, K.Y. Lam, K.M. Liew, J.N. Reddy, Dynamic stability analysis of functionally graded cylindrical shells under periodic axial loading, *International Journal of Solids and Structures* 38 (2001) 1295–1309.

[17] J. Yang, H.-S. Shen, Vibration characteristics and transient response of shear-deformable functionally graded plates in thermal environments, *Journal of Sound and Vibration* 255 (2002) 579–602.

[18] J. Yang, H.-S. Shen, Free vibration and parametric resonance of shear deformable functionally graded cylindrical panels, *Journal of Sound and Vibration* 261 (2003) 871–893.

[19] B.P. Patel, S.S. Gupta, M.S. Loknath, C.P. Kadu, Free vibration analysis of functionally graded elliptical cylindrical shells using higher-order theory, *Composite Structures* 69 (2005) 259–270.

[20] J. Woo, S.A. Meguid, L.S. Ong, Nonlinear free vibration behavior of functionally graded plates, *Journal of Sound and Vibration* 289 (2006) 595–611.

[21] K.M. Liew, J. Yang, Y.F. Wu, Nonlinear vibration of a coating-FGM-substrate cylindrical panel subjected to a temperature gradient, *Computer Methods in Applied Mechanics and Engineering* 195 (2006) 1007–1026.

[22] C.S. Chen, Nonlinear vibration of a shear deformable functionally graded plate, *Composite Structures* 68 (2005) 295–302.

[23] X.L. Huang, H.-S. Shen, Nonlinear vibration and dynamic response of functionally graded plates in thermal environments, *International Journal of Solids and Structures* 41 (2004) 2403–2427.
[24] N. Sundararajan, T. Prakash, M. Ganapathi, Nonlinear free flexural vibrations of functionally graded rectangular and skew plates under thermal environments, *Finite Elements in Analysis and Design* 42 (2005) 152–168.
[25] X.L. Huang, H.-S. Shen, Vibration and dynamic response of functionally graded plates with piezoelectric actuators in thermal environments, *Journal of Sound and Vibration* 289 (2006) 25–53.
[26] H.-S. Shen, K.M. Liew, Postbuckling of axially loaded functionally graded cylindrical panels with piezoelectric actuators in thermal environments, *Journal of Engineering Mechanics—ASCE* 130 (2004) 982–995.
[27] J. Yang, K.M. Liew, Y.F. Wu, S. Kitipornchai, Thermo-mechanical post-buckling of FGM cylindrical panels with temperature-dependent properties, *International Journal of Solids and Structures* 43 (2006) 307–324.
[28] H.-S. Shen, A.Y.T. Leung, Postbuckling of pressure-loaded functionally graded cylindrical panels in thermal environments, *Journal of Engineering Mechanics—ASCE* 129 (2003) 414–425.
[29] Y.W. Kim, Temperature dependent vibration analysis of functionally graded rectangular plates, *Journal of Sound and Vibration* 284 (2005) 531–549.
[30] J.S. Park, J.H. Kim, Thermal postbuckling and vibration analyses of functionally graded plates, *Journal of Sound and Vibration* 289 (2006) 77–93.
[31] R. Kadoli, N. Ganesan, Buckling and free vibration analysis of functionally graded cylindrical shells subjected to a temperature-specified boundary condition, *Journal of Sound and Vibration* 289 (2006) 450–480.
[32] H.-S. Shen, N. Noda, Postbuckling of FGM cylindrical shells under combined axial and radial mechanical loads in thermal environments, *International Journal of Solids and Structures* 42 (2005) 4641–4662.
[33] T. Kant, R.K. Khare, A higher-order facet quadrilateral composite shell element, *International Journal for Numerical Methods in Engineering* 40 (1997) 4477–4499.
[34] R.K. Khare, T. Kant, A.K. Garg, Free vibration of composite and sandwich laminates with a higher-order facet shell element, *Composite Structures* 65 (2004) 405–418.
[35] S.S. Vel, R.C. Batra, Three-dimensional exact solution for the vibration of functionally graded rectangular plates, *Journal of Sound and Vibration* 272 (2004) 703–730.
[36] H. Matsunaga, Free vibration and stability of functionally graded plates according to a 2-D higher-order deformation theory, *Composite Structures* 82 (2008) 499–512.
[37] A.J.M. Ferreira, R.C. Batra, C.M.C. Roque, L.F. Qian, R.M.N. Jorge, Natural frequencies of functionally graded plates by meshless method, *Composite Structures* 75 (2006) 593–600.
[38] L.F. Qian, R.C. Batra, L.M. Chen, Static and dynamic deformations of thick functionally graded elastic plate by using higher-order shear and normal deformable plate theory and meshless local Petrov–Galerkin method, *Composites: Part B* 35 (2004) 685–697.
[39] T.Y. Ng, K.Y. Lam, J.N. Reddy, Dynamic stability of cylindrical panels with transverse shear effects, *International Journal of Solids and Structures* 36 (1999) 3483–3496.